Korea-Australia Rheology Journal, 29(4), 303-316 (November 2017) www.springer.com/13367
DOI: 10.1007/s13367-017-0030-2

Numerical modelling on pulsatile flow of Casson nanofluid through an inclined artery with stenosis and tapering under the influence of magnetic field and periodic body acceleration

R. Ponalagusamy* and S. Priyadharshini
Department of Mathematics, National Institute of Technology, Tiruchirappalli 620015, India
(Received May 25, 2017; final revision received July 24, 2017; accepted August 10, 2017)

The present study investigates the pulsatile flow of Casson nanofluid through an inclined and stenosed artery with tapering in the presence of magnetic field and periodic body acceleration. The iron oxide nanoparticles are allowed to flow along with it. The governing equations for the flow of Casson fluid when the artery is tapered slightly having mild stenosis are highly non-linear and the momentum equations for temperature and concentration are coupled and are solved using finite difference numerical schemes in order to find the solutions for velocity, temperature, concentration, wall shear stress, and resistance to blood flow. The aim of the present study is to analyze the effects of flow parameters on the flow of nanofluid through an inclined arterial stenosis with tapering. These effects are represented graphically and concluded that the wall shear stress profiles enhance with increase in yield stress, magnetic field, thermophoresis parameter and decreases with Brownian motion parameter, local temperature Grashof number, local nanoparticle Grashof number. The significance of the model is the existence of yield stress and it is examined that when the rheology of blood changes from Newtonian to Casson fluid, the percentage of decrease in the flow resistance is higher with respect to the increase in the parameters local temperature Grashof number, local nanoparticle Grashof number, Brownian motion parameter, and Prandtl number. It is pertinent to observe that increase in the Brownian motion parameter leads to increment in concentration and temperature profiles. It is observed that the concentration of nanoparticles decreases with increase in the value of thermophoresis parameter.

Keywords: nanofluid, stenosis, tapering, thermophoresis, Brownian motion, Casson fluid

1. Introduction

Stenosis in an artery is defined as a narrowing of artery caused by the deposition of fatty substances on the arterial wall resisting blood flow to the organs resulting in severe cardiovascular diseases. The understanding of hemodynamical factors is essential in order to study the process of diagnosis and treatment of various cardiovascular diseases (Caro, 1982; Ku, 1997; Shukla *et al.*, 1980; Ponalagusamy, 1986; Young, 1968; 1979; Young and Tsai, 1973). The flow of blood through arteries has been investigated treating blood as Newtonian fluid (Chaturani and Ponnalagarsamy, 1984; El-Shahed, 2003; Elshehawey *et al.*, 2000; Sharma *et al.*, 2012). Liu *et al.* (2004) analysed numerically the effects of pulsatility, stenosis, and tapering on blood flow and found that the maximum magnitude of wall shear stress is larger for a artery with tapering than artery without tapering. Chakravarty and Mandal (2000) and Mandal (2005) analysed Newtonian and non-Newtonian flows through tapered arterial stenosis. Mekheimer and El Kot (2008) analysed the effects of taper angle on flow of blood an artery with tapering and stenosis by considering blood as micropolar fluid. Jeffords and Knisley (1956) and Bloch (1962) investigated the effects of tapering on hydrodynamic factors such as shear stress at the wall, volumetric flow rate, and resistive impedance. The red blood cells or erythrocytes in the blood form a rod shaped stack of cells called rouleux at low shear stress. The structure is disturbed when a finite amount of stress is applied. The finite amount of stress is known as yield stress. When the applied shear stress is less than the yield stress, the fluid behaves as a solid plug. The existence of yield stress due to the red blood cells in the blood has been explained (Nguyen and Boger, 1992; Rodkiewicz *et al.*, 1990). Hence it is worthful to consider the effects of yield stress on blood flow in the present investigation. Several investigators (Blair, 1959; Charm and Kurland, 1965; Merrill *et al.*, 1965) have shown experimentally that blood behaves like a Casson fluid. Blair and Spanner (1974) suggested that the rheology of blood can be taken as Casson fluid. In studies by Siddiqui *et al.* (2009) and Chaturani and Ponalagusamy (1986), the flow of blood through arterial stenosis assuming it as Casson fluid has been investigated.

Magnetohydrodynamics deals with the interaction of magnetic fields with the electrically conducting fluids in motion. Magnet therapy has been used in medical field to cure severe aches, to control blood flow during surgeries

*Corresponding author; E-mail: rpalagu@nitt.edu

and in tissue engineering. Hence it is pertinent to study the effects of MHD on the flow of blood through stenosed artery. Bali and Awasthi (2012) investigated the influence of external magnetic field on blood flow assuming blood as Casson fluid. Akbar (2015) brought out the MHD effects on Casson fluid and its applications in crude oil refinement. Chaturani and Palanisamy (1990) dealt with the flow of Casson fluid in the presence of body acceleration. El-shahed (2003) analysed the effects of periodic body acceleration on pulsatile flow of blood as Newtonian fluid through an artery with stenosis. Dash *et al.* (1996) analysed the Casson fluid flow through a tube taking the effects of permeability into effect. Sharma *et al.* (2012) investigated the pulsatile flow of blood through an artery with stenosis.

Nanofluid is a fluid containing nanoparticles of size 1-100 nm uniformly distributed in a base fluid. Nanofluids have an important feature *i.e.* its higher thermal conductivity. Nanofluids are stable over months. Nanofluids have gained significant attention from researchers due to its enhanced thermal properties. Nanoparticles possess antibacterial properties and are capability to deliver drugs to a targeted site, hence nanofluids with nanoparticles also has similar properties and are used in the process of drug delivery in cancer treatments. Magnetic nanofluids are used to drive the particles in the blood stream to the tumour cells with the use of magnets. There are various applications of nanofluids in biomedicine such as magnetic cell separation, hyperthermia and MRIs. Nanofluids are applied in the treatment of several diseases by modifying the properties of nanoparticles. The advantage of using nanoparticles as delivery vehicles for drug delivery is that the living cells absorb them when they reach the cell's surface due to its small size. Nanofluids are used in industries in the process of heat transfer and heat exchanging devices.

Choi and Eastman (1995) introduced the new class of nanotechnology on the basis of heat transfer fluids. Nadeem and Ijaz (2015) analysed the influence of the metallic nanoparticles on blood flow through curved arteries with tapering. The flow of nanofluid and its applications have been extensively studied by Nadeem and Ijaz (2015). Akbar and Butt (2015) investigated the MHD effects and copper nanoparticles on blood flow through arteries having composite stenosis. Ellahi (2013) analysed the effects of non-Newtonian characteristics on nanofluid flow in a pipe. The analytical solutions are obtained for the velocity field, the temperature distribution, and nano concentration by solving the nonlinear partial differential equations with the boundary conditions using homotopy analysis method (HAM). Ellahi *et al.* (2014) studied the effects of slip parameter on the blood flow treating blood as Jeffrey nanofluid through an artery with composite stenosis. Further the momentum equations are solved using Homotopy Perturbation Method (HPM) to find the steady state solutions. Nadeem *et al.* (2014) investigated the MHD flow of Prandtl nanofluid through a stenosed artery. In all the above studies, steady flow of nanofluid has been analysed.

Rahman *et al.* (2016) have analysed the effects of nanoparticles on Jeffrey fluid through tapered artery with mild stenosis. The solutions of the problem are obtained using HPM and found that Grashof number and mild stenosis have same effects on impedance. Mamourian *et al.* (2016) have investigated a two dimensional model for sensitive analysis of combined turbulent mixed convection and radiation heat transfer using two phase mixture in a solar heat exchanger where numerical simulations were carried out to study the effects of parameters such as volume fraction of nanoparticles and nanoparticles diameter. Shehzad *et al.* (2016) have discussed the simultaneous effects of Brownian motion and thermophoresis using the Buongiorno's mathematical model. Sheikholeslami *et al.* (2016) have investigated the influence of induced magnetic field on free convection of nanofluid by taking into account the impact of Brownian motion and the properties of nanofluid.

Ellahi *et al.* (2016) have studied the effects of nanoparticles on shear stress, heat flux, and thermal resistance through a model on mixed convection flow of power law fluid. Hayat *et al.* (2017) have analysed the features including thermophoresis and Brownian motion in the model on squeezing flow of couple stress nanofluid. Rashidi *et al.* (2017) have developed a discrete phase model to analyse the nature of aluminium oxide nanoparticles taking Brownian, drag, gravity, and thermophoresis forces into account. Hariri *et al.* (2017) have investigated the effects of non-uniform magnetic field and heat transfer on flow of ferrofluid in a tube. Ibrahim *et al.* (2017) have analysed the mathematical model for mixed convection on MHD flow of Casson fluid and observed that Casson fluid parameter is helpful in minimizing skin friction. An unsteady flow of nanofluid in an inclined stenosed artery with tapering under the influence of magnetic field and periodic acceleration has not been explored so far. Motivated by all these, the aim of the present study is to analyse the MHD effects on the pulsatile flow of Casson nanofluid through an inclined arterial stenosis with external magnetic field and periodic body acceleration.

2. Mathematical Formulation

Consider an incompressible, laminar, unsteady blood flow through an inclined artery with tapering and stenosis inclined at an angle β under the influence of periodic body acceleration where blood is treated as Casson nanofluid and iron oxide nanoparticles are also flowing along with it. An external magnetic field $\overline{B}_0^2$ acts perpendicular to the

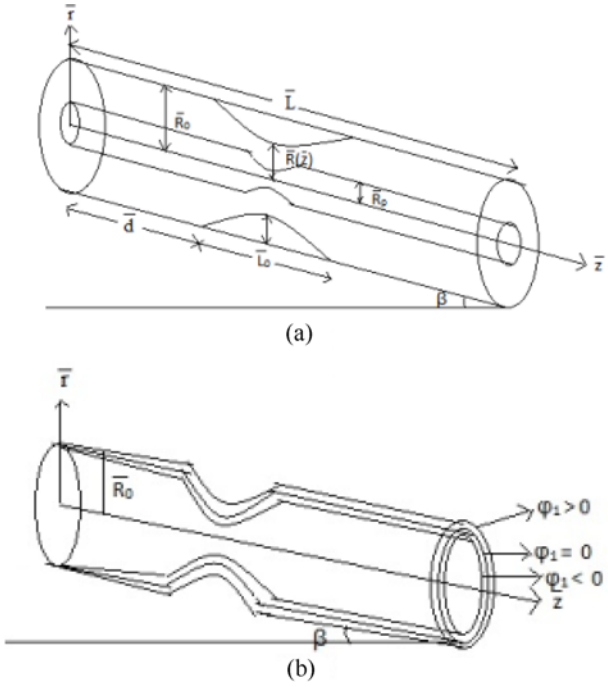

Fig. 1. (a) Geometry of inclined artery with stenosis and plug core region. (b) Geometry of inclined artery with tapering.

axis. The cylindrical coordinates $(\bar{r},\bar{\theta},\bar{z})$ is used to denote a point in a system where $\bar{z}$-axis is considered as the axis of the artery, $\bar{r}$ denotes the radial direction, and $\bar{\theta}$ represents the circumferential direction (Fig. 1). The walls of the artery are maintained at temperature $\bar{T}_1$ and concentration $\bar{C}_1$ to analyse the effects of heat and mass transfer. The velocity, temperature, and concentration distributions are symmetric at the centre of the tube.

The momentum equations for pulsatile flow of Casson nanofluid with heat and mass transfer through an inclined artery in the presence of external magnetic field and periodic body acceleration are given by the following (Ellahi *et al.*, 2014; Nadeem and Ijaz, 2015):

$$\frac{1}{\bar{r}}\frac{\partial}{\partial \bar{r}}(\bar{r}\bar{v})+\frac{\partial \bar{u}}{\partial \bar{z}}=0\,, \tag{1}$$

$$\begin{aligned}&\bar{\rho}_f\left[\frac{\partial \bar{u}}{\partial \bar{t}}+\bar{u}\frac{\partial \bar{u}}{\partial \bar{z}}+\bar{v}\frac{\partial \bar{u}}{\partial \bar{r}}\right]=\\&-\frac{\partial \bar{p}}{\partial \bar{z}}+\bar{\rho}_f\bar{g}\sin\beta+\frac{1}{\bar{r}}\frac{\partial}{\partial \bar{r}}(\bar{r}\bar{\tau}_{rz})+\frac{\partial}{\partial \bar{z}}(\bar{\tau}_{zz})\\&-\bar{\sigma}\bar{B}_0^2\bar{u}+\bar{\rho}_f\bar{g}\bar{\alpha}_t(\bar{T}-\bar{T}_1)+\bar{\rho}_f\bar{g}\bar{\alpha}_c(\bar{C}-\bar{C}_1)+\bar{\rho}_f\bar{F}(\bar{t}),\end{aligned} \tag{2}$$

$$\begin{aligned}&\bar{\rho}_f\left[\frac{\partial \bar{v}}{\partial \bar{t}}+\bar{u}\frac{\partial \bar{v}}{\partial \bar{z}}+\bar{v}\frac{\partial \bar{v}}{\partial \bar{r}}\right]=\\&-\frac{\partial \bar{p}}{\partial \bar{r}}-\bar{\rho}_f\bar{g}\cos\beta+\frac{1}{\bar{r}}\frac{\partial}{\partial \bar{r}}(\bar{r}\bar{\tau}_{rr})+\frac{\partial}{\partial \bar{z}}(\bar{\tau}_{rz})-\frac{\bar{\tau}_{\theta\theta}}{\bar{r}},\end{aligned} \tag{3}$$

$$\begin{aligned}&\frac{\partial \bar{T}}{\partial \bar{t}}+\bar{v}\frac{\partial \bar{T}}{\partial \bar{r}}+\bar{u}\frac{\partial \bar{T}}{\partial \bar{z}}=\bar{\zeta}\left(\frac{\partial^2\bar{T}}{\partial \bar{r}^2}+\frac{1}{\bar{r}}\frac{\partial \bar{T}}{\partial \bar{r}}+\frac{\partial^2\bar{T}}{\partial \bar{z}^2}\right)\\&+\eta\left[D_{\bar{B}}\left(\frac{\partial \bar{C}}{\partial \bar{r}}\frac{\partial \bar{T}}{\partial \bar{r}}+\frac{\partial \bar{C}}{\partial \bar{z}}\frac{\partial \bar{T}}{\partial \bar{z}}\right)+\frac{D_{\bar{T}}}{\bar{T}_0}\left(\left(\frac{\partial \bar{T}}{\partial \bar{r}}\right)^2+\left(\frac{\partial \bar{T}}{\partial \bar{z}}\right)^2\right)\right],\end{aligned} \tag{4}$$

$$\begin{aligned}&\frac{\partial \bar{C}}{\partial \bar{t}}+\bar{v}\frac{\partial \bar{C}}{\partial \bar{r}}+\bar{u}\frac{\partial \bar{C}}{\partial \bar{z}}=D_{\bar{B}}\left(\frac{\partial^2\bar{C}}{\partial \bar{r}^2}+\frac{1}{\bar{r}}\frac{\partial \bar{C}}{\partial \bar{r}}+\frac{\partial^2\bar{C}}{\partial \bar{z}^2}\right)\\&+\frac{D_{\bar{T}}}{\bar{T}_0}\left(\frac{\partial^2\bar{T}}{\partial \bar{r}^2}+\frac{1}{\bar{r}}\frac{\partial \bar{T}}{\partial \bar{r}}+\frac{\partial^2\bar{T}}{\partial \bar{z}^2}\right)\end{aligned} \tag{5}$$

where the stress components are given as (Shaw *et al.*, 2010)

$$\bar{\tau}_{zz}=2\bar{\mu}(\bar{J}_2)\left(\frac{\partial \bar{u}}{\partial \bar{z}}\right), \tag{6}$$

$$\bar{\tau}_{rr}=2\bar{\mu}(\bar{J}_2)\left(\frac{\partial \bar{v}}{\partial \bar{r}}\right), \tag{7}$$

$$\bar{\tau}_{rz}=\bar{\mu}(\bar{J}_2)\left(\frac{\partial \bar{u}}{\partial \bar{r}}+\frac{\partial \bar{v}}{\partial \bar{z}}\right), \tag{8}$$

$$\bar{\mu}(\bar{J}_2)=(\bar{\mu}_c^{\frac{1}{2}}\bar{J}_2^{\frac{1}{4}}+2^{-\frac{1}{2}}\bar{\tau}_y^{\frac{1}{2}})^2\bar{J}_2^{-\frac{1}{2}}\ \text{with} \tag{9}$$

$$\bar{J}_2=2\left\{\left(\frac{\partial \bar{v}}{\partial \bar{r}}\right)^2+\left(\frac{\bar{v}}{\bar{r}}\right)^2+\left(\frac{\partial \bar{u}}{\partial \bar{z}}\right)^2\right\}+\left(\frac{\partial \bar{v}}{\partial \bar{z}}+\frac{\partial \bar{u}}{\partial \bar{r}}\right)^2. \tag{10}$$

$\bar{u},\bar{v}$ are the velocities along axial and radial directions respectively, $\bar{z}$ denotes the axial distance, $\bar{r}$ represents the radial direction, $\bar{t}$ is the time, $\bar{p}$ is the pressure, $\bar{\rho}_f$ is the density of fluid, β is the inclination angle, $\bar{\sigma}$ is the electrical conductivity of the fluid, $\bar{B}_0$ denotes the strength of magnetic field, $\bar{\alpha}_t$ and $\bar{\alpha}_c$ are the coefficients of thermal expansion and thermal expansion with nanoconcentration, respectively, $\bar{\mu}_c$ represents the Casson's viscosity, $\bar{T}$ denotes the temperature of the fluid, $\bar{C}$ represents the concentration of nanoparticles, $\eta=\frac{(\bar{\rho c})_p}{(\bar{\rho c})_f}$ is the ratio of the effective heat capacity of the nanoparticle to the heat capacity of the fluid, $\bar{c}$ being the volumetric expansion coefficient, the thermal diffusivity $\bar{\zeta}=\frac{\bar{k}_f}{(\bar{\rho c})_f}$, $\bar{k}_f$ denotes the effective thermal conductivity of the nanofluid, $D_{\bar{B}}$ is the Brownian diffusion coefficient, $D_{\bar{T}}$ is the thermospheric diffusion coefficient, $\bar{T}_0$ and $\bar{C}_0$ are initial temperature of the nanofluid and initial concentration of nanoparticles, respectively, the body acceleration per unit mass is expressed as $\bar{F}(\bar{t})=\bar{A}cos(\bar{\omega}_1\bar{t}+\varphi)$, $\bar{A}$ is the constant amplitude of periodic body acceleration, ϕ is the phase angle of body acceleration and $\bar{\omega}_1=2\pi\bar{f}_1$, $\bar{f}_1$ is the

frequency of body acceleration which is assumed to be negligible and hence the wave effects can be eliminated, $\bar{\mu}(\bar{J}_2)$ is the apparent viscosity, and $\bar{\tau}_y$ denotes the yield stress of Casson fluid. ('–' over the letter denotes the corresponding dimensional quantity).

The nature of blood flow is pulsatile and the pressure gradient in dimensional form is expressed as (Shaw *et al.*, 2010)

$$-\frac{\partial \bar{p}}{\partial \bar{z}} = \bar{A}_0 + \bar{A}_1 \cos \bar{\omega} \bar{t} \tag{11}$$

where $\bar{A}_0$ is the amplitude of the steady state pressure gradient, $\bar{A}_1$ is the amplitude of the pulsatile pressure gradient, and the angular frequency $\bar{\omega}$ is expressed as $\bar{\omega} = 2\pi \bar{f}$ where $\bar{f}$ is the frequency of pulse.

The flow conditions for Casson fluid are given as (Shaw *et al.*, 2010)

$$\bar{e}_{ij} = \begin{cases} 0 & \text{if } \bar{J}_2^* < \bar{\tau}_y^{\,2} \\ \dfrac{1}{2}\bar{\mu}(\bar{J}_2)\bar{\tau}_{ij} & \text{if } \bar{J}_2^* \geq \bar{\tau}_y^{\,2} \end{cases} \tag{12}$$

where $\bar{J}_2^* = \dfrac{1}{2}\bar{\tau}_{ij}\bar{\tau}_{ij}$ denotes the second invariant of the stress tensor and $\bar{J}_2 = \dfrac{1}{2}\bar{e}_{ij}\bar{e}_{ij}$ is the rate of strain tensor invariant.

The initial conditions are given as follows:

$$\bar{u} = 0,\ \bar{T} = \bar{T}_0,\ \bar{C} = \bar{C}_0 \text{ at } \bar{t} = 0 \tag{13}$$

and the boundary conditions are given by (Ellahi *et al.*, 2014)

$$(i)\ \frac{\partial \bar{u}}{\partial \bar{r}} = 0 \text{ on } \bar{r} = \bar{R}_p, \tag{14}$$

$$(ii)\ \frac{\partial \bar{T}}{\partial \bar{r}} = 0,\ \frac{\partial \bar{C}}{\partial \bar{r}} = 0 \text{ on } \bar{r} = 0, \tag{15}$$

$$(iii)\ \bar{u} = 0,\ \bar{T} = \bar{T}_1,\ \bar{C} = \bar{C}_1 \text{ on } \bar{r} = \bar{R}(\bar{z}) \tag{16}$$

where R_p is the radius of plug core region.

The flow geometry of the stenosed artery with tapering is defined as (Ponalagusamy and Tamil Selvi, 2013)

$$\bar{R}(\bar{z}) = \begin{cases} (\bar{R}_0 - \psi \bar{z})\left[1 - \bar{B}\left\{\bar{L}_0(\bar{z} - \bar{d}) - (\bar{z} - \bar{d})^2\right\}\right], \bar{d} \leq \bar{z} \leq \bar{d} + \bar{L}_0 \\ (\bar{R}_0 - \psi \bar{z}) \quad \text{otherwise} \end{cases} \tag{17}$$

where $\bar{B} = \dfrac{4\bar{\delta}_s}{\bar{R}_0 \bar{L}_0^2}$, $\bar{R}(\bar{z})$ represents the radius of a tapered arterial stenosis, $\bar{\delta}_s$ is the maximum height of stenosis, ψ denotes the tapering parameter, $\bar{d}$ indicates the location of stenosis, $\bar{R}_0$ is the radius of the normal artery, and $\bar{L}_0$ represents the stenotic length. The tapering parameter $\psi = \tan\phi_1$, ϕ_1 is the taper angle. It is pertinent to note that ϕ_1 is greater than zero for converging tapered artery, $\phi_1 < 0$ indicates the diverging tapered artery and $\phi_1 = 0$ for stenosed artery without tapering.

The followings are the non-dimensional quantities:

$$r = \frac{\bar{r}}{\bar{R}_0},\ z = \frac{\bar{z}}{\bar{R}_0},\ u = \frac{\bar{u}}{\bar{u}_0},\ v = \frac{\bar{L}_0 \bar{v}}{\bar{u}_0 \bar{\delta}_s},\ p = \frac{\bar{R}_0 \bar{p}}{\bar{u}_0 \bar{\mu}_c},\ \tau_{rr} = \frac{\bar{L}_0 \bar{\tau}_{rr}}{\bar{u}_0 \bar{\mu}_c},\ \tau_{rz} = \frac{\bar{R}_0 \bar{\tau}_{rz}}{\bar{u}_0 \bar{\mu}_c},$$
$$\tau_{zz} = \frac{\bar{L}_0 \bar{\tau}_{zz}}{\bar{u}_0 \bar{\mu}_c},\ \tau_{\theta\theta} = \frac{\bar{L}_0 \bar{\tau}_{\theta\theta}}{\bar{u}_0 \bar{\mu}_c},\ \tau_y = \frac{\bar{R}_0 \bar{\tau}_y}{\bar{u}_0 \bar{\mu}_c},\ \alpha^2 = \frac{\bar{\rho}_f \bar{\omega} \bar{R}_0^2}{\bar{\mu}_c},\ M^2 = \frac{\bar{\sigma} \bar{B}_0^2 \bar{R}_0^2}{\bar{\mu}_c},$$
$$Gr = \frac{\bar{\rho}_f \bar{g} \bar{\alpha}_t \bar{R}_0^2 (\bar{T}_0 - \bar{T}_1)}{\bar{\mu}_c \bar{u}_0},\ Br = \frac{\bar{\rho}_f \bar{g} \bar{\alpha}_c \bar{R}_0^2 (\bar{C}_0 - \bar{C}_1)}{\bar{\mu}_c \bar{u}_0},\ Pr = \frac{\bar{\nu}}{\bar{\zeta}},\ Sc = \frac{\bar{\nu}}{D_{\bar{B}}},$$
$$Nt = \frac{(\overline{\rho c})_p D_{\bar{T}} (\bar{T}_0 - \bar{T}_1)}{(\overline{\rho c})_f \bar{T}_0 \bar{\nu}},\ Nb = \frac{(\overline{\rho c})_p D_{\bar{B}} (\bar{C}_0 - \bar{C}_1)}{(\overline{\rho c})_f \bar{\nu}}, \tag{18}$$
$$\bar{\nu} = \frac{\bar{\mu}_c}{\bar{\rho}_f},\ \bar{T} = \bar{T}_1 + (\bar{T}_0 - \bar{T}_1)T,\ \bar{C} = \bar{C}_1 + (\bar{C}_0 - \bar{C}_1)C,\ A_0 = \frac{\bar{R}_0^2 \bar{A}_0}{\bar{u}_0 \bar{\mu}_c},$$
$$A_1 = \frac{\bar{R}_0^2 \bar{A}_1}{\bar{u}_0 \bar{\mu}_c},\ t = \bar{t}\,\bar{\omega},\ A = \frac{\bar{\rho}_f \bar{R}_0^2 \bar{A}}{\bar{u}_0 \bar{\mu}_c},\ A_2 = \frac{\bar{\rho}_f \bar{g} \bar{R}_0^2}{\bar{u}_0 \bar{\mu}},\ \omega_1 = \frac{\bar{\omega}_1}{\bar{\omega}}$$

where $\bar{u}_0$ denotes the average velocity of flow in the uniform artery, $\bar{\rho}$ is the density of nanofluid, α^2 is the Womersley number, M is the Hartmann number, $Re = \dfrac{\bar{\rho} \bar{u}_0 \bar{R}_0}{\bar{\mu}_c}$ is the Reynolds number, Nt, Nb, Gr, Br, Pr, and Sc are the thermophoresis parmeter, the Brownian motion parameter, local temperature Grashof number, local nanoparticle Grashof number, Prandtl number, and Schmidt number, respectively.

Under the non-dimensionalization Eq. (18), the momentum equations governing the pulsatile flow of Casson nanofluid through an inclined artery with slight tapering artery and mild stenosis $\left(\dfrac{\bar{\delta}_s}{\bar{R}_0} << 1, \dfrac{\bar{\delta}_s}{\bar{L}_0} << 1\right)$ prone to the following conditions (Mekheimer and El Kot, 2008) $(i)\ \dfrac{Re\bar{\delta}_s}{\bar{L}_0} << 1, (ii)\ \dfrac{\bar{R}_0}{\bar{L}_0} \sim 0(1)$ are

$$\alpha^2 \frac{\partial u}{\partial t} = -\frac{\partial p}{\partial z} + A_2 \sin\beta + \frac{1}{r}\frac{\partial}{\partial r}(r\tau) - M^2 u + F(t) + GrT + BrC, \tag{19}$$

$$\alpha^2 \frac{\partial T}{\partial t} = \frac{1}{Pr}\left(\frac{\partial^2 T}{\partial r^2} + \frac{1}{r}\frac{\partial T}{\partial r}\right) + \frac{Nb}{Pr}\frac{\partial C}{\partial r}\frac{\partial T}{\partial r} + \frac{Nt}{Pr}\left(\frac{\partial T}{\partial r}\right)^2, \tag{20}$$

$$\alpha^2 \frac{\partial C}{\partial t} = \frac{1}{Sc}\left(\frac{\partial^2 C}{\partial r^2} + \frac{1}{r}\frac{\partial C}{\partial r}\right) + \frac{Nt}{ScNb}\left(\frac{\partial^2 T}{\partial r^2} + \frac{1}{r}\frac{\partial T}{\partial r}\right) \tag{21}$$

with initial conditions

$$u = 0,\ T = 1,\ C = 1 \text{ at } t = 0 \tag{22}$$

and boundary conditions

$$(i)\ \frac{\partial u}{\partial r}=0 \text{ at } r=R_p, \tag{23}$$

$$(ii)\ \frac{\partial T}{\partial r}=0,\ \frac{\partial C}{\partial r}=0 \text{ at } r=0, \tag{24}$$

$$(iii)\ u=0,\ T=0,\ C=0 \text{ at } r=R(z). \tag{25}$$

The corresponding dimensionless characteristic equation of casson fluid is given by Shaw *et al.* (2009)

$$\begin{aligned}&\tau^{\frac{1}{2}}=\tau_y^{\frac{1}{2}}+\left(\frac{\partial u}{\partial r}\right)^{\frac{1}{2}},\ \tau\geq\tau_y\\&\frac{\partial u}{\partial r}=0,\ \tau<\tau_y\end{aligned}. \tag{26}$$

The geometry of tapered arterial stenosis in non-dimensional form is expressed as

$$R(z)=\begin{cases}(1-\psi z)[1-B\{L_0(z-d)-(z-d)^2\}], d\leq z\leq d+L_0\\(1-\psi z)\text{ otherwise}\end{cases} \tag{27}$$

where $B=\frac{4\delta_s}{L_0^2}$.

Differentiating partially Eq. (19) with respect to 'r' and using Eq. (26), we get

$$\begin{aligned}\alpha^2(1-\tau^{-\frac{1}{2}}\tau_y^{\frac{1}{2}})\frac{\partial\tau}{\partial t}&=\frac{\partial^2\tau}{\partial r^2}+\frac{1}{r}\frac{\partial\tau}{\partial r}-\frac{\tau}{r^2}\\&-M^2(\tau-2\tau^{\frac{1}{2}}\tau_y^{\frac{1}{2}}+\tau_y)+Gr\frac{\partial T}{\partial r}+Br\frac{\partial C}{\partial r}.\end{aligned} \tag{28}$$

3. Solution

Let us use the radial coordinate transformation $\xi=\frac{r}{R}$. Then $\frac{\partial}{\partial t}=\frac{\partial}{\partial t}$, $\frac{\partial}{\partial r}=\frac{1}{R}\frac{\partial}{\partial\xi}$, $\frac{\partial^2}{\partial r^2}=\frac{1}{R^2}\frac{\partial^2}{\partial\xi^2}$. Therefore the Eqs. (28), (20), and (21) become

$$\begin{aligned}\alpha^2(1-\tau^{-\frac{1}{2}}\tau_y^{\frac{1}{2}})\frac{\partial\tau}{\partial t}&=\frac{1}{R^2}\frac{\partial^2\tau}{\partial\xi^2}+\frac{1}{R^2\xi}\frac{\partial\tau}{\partial\xi}-\frac{\tau}{R^2\xi^2}\\&-M^2(\tau-2\tau^{\frac{1}{2}}\tau_y^{\frac{1}{2}}+\tau_y)+\frac{Gr}{R}\frac{\partial T}{\partial\xi}+\frac{Br}{R}\frac{\partial C}{\partial\xi}\end{aligned}, \tag{29}$$

$$\alpha^2\frac{\partial T}{\partial t}=\frac{1}{R^2}\left[\frac{1}{Pr}\left(\frac{\partial^2T}{\partial\xi^2}+\frac{1}{\xi}\frac{\partial T}{\partial\xi}\right)+Nb\frac{\partial C}{\partial\xi}\frac{\partial T}{\partial\xi}+Nt\left(\frac{\partial T}{\partial\xi}\right)^2\right], \tag{30}$$

$$\alpha^2\frac{\partial C}{\partial t}=\frac{1}{ScR^2}\left[\left(\frac{\partial^2C}{\partial\xi^2}+\frac{1}{\xi}\frac{\partial C}{\partial\xi}\right)+\frac{Nt}{Nb}\left(\frac{\partial^2T}{\partial\xi^2}+\frac{1}{\xi}\frac{\partial T}{\partial\xi}\right)\right] \tag{31}$$

with the following initial conditions

$$\tau=\beta_1(\beta_1<<1),\ T=1,\ C=1 \text{ at } t=0 \tag{32}$$

and boundary conditions in terms of shear stress are

$$(i)\ \tau=0,\ \frac{\partial T}{\partial\xi}=0,\ \frac{\partial C}{\partial\xi}=0 \text{ at } \xi=0, \tag{33}$$

$$(ii)\ \frac{1}{R}\frac{\partial\tau}{\partial\xi}+\frac{\tau}{R\xi}=f(t),\ T=0,\ C=0 \text{ at } \xi=1 \tag{34}$$

where $f(t)=-A_0-A_1\cos(t)-A_2\sin(\beta)-A\cos(\omega_1 t+\varphi)$.

To solve Eqs. (29), (30), and (31) with Eqs. (32) to (34), we apply finite difference schemes as follows:

$$\begin{aligned}&\frac{\partial\tau}{\partial t}=\frac{\tau_{i,j}^{(n+1)}-\tau_{i,j}^{(n)}}{\Delta t},\ \frac{\partial T}{\partial t}=\frac{T_{i,j}^{(n+1)}-T_{i,j}^{(n)}}{\Delta t},\ \frac{\partial C}{\partial t}=\frac{C_{i,j}^{(n+1)}-C_{i,j}^{(n)}}{\Delta t},\\&\frac{\partial\tau}{\partial\xi}=\frac{\tau_{i,j+1}^{(n)}-\tau_{i,j-1}^{n}}{2\Delta\xi},\ \frac{\partial T}{\partial\xi}=\frac{T_{i,j+1}^{(n)}-T_{i,j-1}^{(n)}}{2\Delta\xi},\ \frac{\partial C}{\partial\xi}=\frac{C_{i,j+1}^{(n)}-C_{i,j-1}^{(n)}}{2\Delta\xi},\\&\frac{\partial^2\tau}{\partial\xi^2}=\frac{\tau_{i,j+1}^{(n)}-2\tau_{i,j}^{(n)}+\tau_{i,j-1}^{(n)}}{(\Delta\xi)^2},\ \frac{\partial^2T}{\partial\xi^2}=\frac{T_{i,j+1}^{(n)}-2T_{i,j}^{(n)}+T_{i,j-1}^{(n)}}{(\Delta\xi)^2},\\&\frac{\partial^2C}{\partial\xi^2}=\frac{C_{i,j+1}^{(n)}-2C_{i,j}^{(n)}+C_{i,j-1}^{(n)}}{(\Delta\xi)^2},\ \tau=\tau_{i,j}^{(n)},\ T=T_{i,j}^{(n)},\ C=C_{i,j}^{(n)}.\end{aligned} \tag{35}$$

Using Eq. (35), Eq. (29) becomes

$$\begin{aligned}\tau_{i,j}^{(n+1)}=\tau_{i,j}^{(n)}+\frac{\Delta t}{\alpha^2(1-\tau_{i,j}^{-\frac{1}{2}}\tau_y^{\frac{1}{2}})}\Bigg[&\frac{1}{R_i^2}\left(\frac{\tau_{i,j+1}^{(n)}-2\tau_{i,j}^{(n)}+\tau_{i,j-1}^{(n)}}{(\Delta\xi)^2}\right)\\&+\frac{1}{R_i^2\xi_j}\left(\frac{\tau_{i,j+1}^{(n)}-\tau_{i,j-1}^{(n)}}{2\Delta\xi}\right)-\frac{\tau_{i,j}^{(n)}}{R_i^2\xi_j^2}-M^2(\tau_{i,j}^{(n)}-2\tau_{i,j}^{(n)\frac{1}{2}}\tau_y^{\frac{1}{2}}+\tau_y)\\&+\frac{Gr}{R_i}\left(\frac{T_{i,j+1}^{(n)}-T_{i,j-1}^{(n)}}{2\Delta\xi}\right)+\frac{Br}{R_i}\left(\frac{C_{i,j+1}^{(n)}-C_{i,j-1}^{(n)}}{2\Delta\xi}\right)\Bigg].\end{aligned} \tag{36}$$

Eq. (30) becomes

$$\begin{aligned}T_{i,j}^{(n+1)}=T_{i,j}^{(n)}+\frac{\Delta t}{\alpha^2R_i^2}\Bigg[&\frac{1}{Pr}\Bigg[\left(\frac{T_{i,j+1}^{(n)}-2T_{i,j}^{(n)}+T_{i,j-1}^{(n)}}{(\Delta\xi)^2}\right)\\&+\frac{1}{\xi_j}\left(\frac{T_{i,j+1}^{(n)}-T_{i,j-1}^{(n)}}{2\Delta\xi)}\right)\Bigg]+Nb\left(\frac{T_{i,j+1}^{(n)}-T_{i,j-1}^{(n)}}{\Delta\xi}\right)\left(\frac{C_{i,j+1}^{(n)}-C_{i,j-1}^{(n)}}{2\Delta\xi}\right)\\&+Nt\left(\frac{T_{i,j+1}^{(n)}-T_{i,j-1}^{(n)}}{2\Delta\xi}\right)^2\Bigg].\end{aligned} \tag{37}$$

Eq. (31) becomes

$$\begin{aligned}C_{i,j}^{(n+1)}=C_{i,j}^{(n)}+\frac{\Delta t}{\alpha^2ScR_i^2}\Bigg[&\left(\frac{C_{i,j+1}^{(n)}-2C_{i,j}^{(n)}+C_{i,j-1}^{(n)}}{(\Delta\xi)^2}\right)\\&+\frac{1}{\xi_j}\left(\frac{C_{i,j+1}^{(n)}-C_{i,j-1}^{(n)}}{2\Delta\xi}\right)+\frac{Nt}{Nb}\Bigg\{\left(\frac{T_{i,j+1}^{(n)}-2T_{i,j}^{(n)}+T_{i,j-1}^{(n)}}{(\Delta\xi)^2}\right)\\&+\frac{1}{\xi_j}\left(\frac{T_{i,j+1}^{(n)}-T_{i,j-1}^{(n)}}{2\Delta\xi}\right)\Bigg\}\Bigg].\end{aligned} \tag{38}$$

The initial conditions are

$$\tau_{i,j}^{(0)} = \beta_1 (\beta_1 << 1),\ T_{i,j}^{(0)} = 1,\ C_{i,j}^{(0)} = 1 \tag{39}$$

and the boundary conditions are

$$(i)\ \tau_{i,0}^{(n+1)} = 0,\ T_{i,0}^{(n+1)} = T_{i,1}^{(n+1)},\ C_{i,0}^{(n+1)} = C_{i,1}^{(n+1)}, \tag{40}$$

$$(ii)\ \tau_{i,N}^{(n+1)} = \frac{1}{1+2\Delta\xi}(\tau_{i,N-2}^{(n+1)} + 2R_i \Delta\xi f(t_{n+1})),\ T_{i,N}^{(n+1)} = 0,\ C_{i,N}^{(n+1)} = 0 \tag{41}$$

where $i = 0,1,2,...,m_1, j = 0,1,...,n_1, z(m_1) = L, \xi(n_1) = 1$.

The initial and boundary conditions in terms of velocity are

$$(i)\ u = 0 \text{ at } t = 0,\ (ii)\ \frac{\partial u}{\partial \xi} = 0 \text{ at } \xi = \xi_p,\ (iii)\ u = 0 \text{ at } \xi = 1 \tag{42}$$

where $\xi_p = \dfrac{r}{R_p}$.

On solving Eq. (36) with initial and boundary conditions Eqs. (39) to (41), shear stress distribution can be obtained. Plug core radius has been calculated from the obtained shear stress distribution. Then the velocity distribution of nanofluid is computed using Eq. (26), initial and boundary conditions (Eq. (42)).

The flow rate is expressed as

$$Q = 2R^2 \left[\int_0^{\xi_p} \xi u d\xi + \int_{\xi_p}^{1} \xi u d\xi \right]. \tag{43}$$

The flow resistance λ is defined as

$$\lambda = \int_0^L \frac{\left(-\dfrac{\partial p}{\partial z}\right)}{Q} dz \tag{44}$$

where L is the length of the artery.

4. Validation

The values of axial velocity are obtained using Finite Difference Method (FDM) and Finite Element Method (FEM) and are tabulated in Tables 1 to 4. The details of the variational FEM can be found in the articles (Beg *et al.*, 2012; Ponnalagarsamy and Kawahara, 1989; Zaman *et al.*, 2017). The numerical solutions for axial velocities are computed using FDM and FEM and are compared in Tables 1 to 4. It is observed that the solutions obtained using both FDM and FEM are in good agreement. This gives the validation of the results obtained using FDM.

5. Discussion

The governing equations of Casson nanofluid are non-linear and solved numerically using finite difference schemes. The flow region is discretized by taking $\Delta\xi =$

Table 1. Numerical values of axial velocity (u) at the midpoint ($z = 5.0$) of the stenotic region for different values of yield stress (θ_1).

ξ	$\theta_1 = 0.0$		$\theta_1 = 0.1$		$\theta_1 = 0.2$	
	FDM	FEM	FDM	FEM	FDM	FEM
0.0	1.8476	1.8474	1.8105	1.8103	1.7743	1.7741
0.1	1.8306	1.8304	1.7987	1.7985	1.7669	1.7667
0.2	1.7757	1.7755	1.7488	1.7486	1.7219	1.7217
0.3	1.6831	1.6830	1.6604	1.6603	1.6376	1.6375
0.4	1.5534	1.5532	1.5341	1.5339	1.5149	1.5147
0.5	1.3867	1.3865	1.3707	1.3705	1.3547	1.3545
0.6	1.1834	1.1832	1.1704	1.1702	1.1574	1.1572
0.7	0.9436	0.9434	0.9335	0.9333	0.9235	0.9233
0.8	0.6670	0.6668	0.6600	0.6598	0.6530	0.6528
0.9	0.3529	0.3527	0.3492	0.3490	0.3455	0.3453
1.0	0	0	0	0	0	0

Table 2. Numerical values of axial velocity (u) at the midpoint ($z = 5.0$) of the stenotic region for different values of Hartmann number (M).

ξ	$M^2 = 0$		$M^2 = 1$		$M^2 = 2$	
	FDM	FEM	FDM	FEM	FDM	FEM
0.0	1.9761	1.9759	1.8105	1.8103	1.6696	1.6694
0.1	1.9626	1.9624	1.7987	1.7985	1.6592	1.6590
0.2	1.9067	1.9065	1.7488	1.7486	1.6142	1.6140
0.3	1.8081	1.8079	1.6604	1.6602	1.5344	1.5342
0.4	1.6678	1.6676	1.5341	1.5339	1.4201	1.4199
0.5	1.4866	1.4864	1.3707	1.3705	1.2716	1.2714
0.6	1.2657	1.2655	1.1704	1.1702	1.0888	1.0886
0.7	1.0059	1.0057	0.9335	0.9333	0.8714	0.8712
0.8	0.7082	0.7080	0.6600	0.6598	0.6186	0.6184
0.9	0.3729	0.3727	0.3492	0.3490	0.3289	0.3287
1.0	0	0	0	0	0	0

Table 3. Numerical values of axial velocity (u) at the midpoint ($z = 5.0$) of the stenotic region for different values of thermophoresis parameter (Nt).

ξ	$Nt = 0.05$		$Nt = 0.1$		$Nt = 0.2$	
	FDM	FEM	FDM	FEM	FDM	FEM
0.0	1.8787	1.8785	1.8105	1.8103	1.6950	1.6948
0.1	1.8663	1.8661	1.7987	1.7985	1.6846	1.6844
0.2	1.8142	1.8140	1.7488	1.7486	1.6395	1.6393
0.3	1.7222	1.7220	1.6604	1.6602	1.5589	1.5587
0.4	1.5908	1.5906	1.5341	1.5339	1.4433	1.4431
0.5	1.4205	1.4203	1.3707	1.3705	1.2927	1.2925
0.6	1.2118	1.2116	1.1704	1.1702	1.1070	1.1068
0.7	0.9653	0.9651	0.9335	0.9333	0.8859	0.8857
0.8	0.6813	0.6811	0.6600	0.6598	0.6287	0.6285
0.9	0.3597	0.3595	0.3492	0.3490	0.3340	0.3338
1.0	0	0	0	0	0	0

Table 4. Numerical values of axial velocity (u) at the midpoint (z = 5.0) of the stenotic region for different values of Brownian motion parameter (Nb).

ξ	N_b = 0.05		N_b = 0.1		N_b = 0.2	
	FDM	FEM	FDM	FEM	FDM	FEM
0.0	1.6958	1.6956	1.8105	1.8103	1.8875	1.8873
0.1	1.6855	1.6853	1.7987	1.7985	1.8749	1.8747
0.2	1.6404	1.6402	1.7488	1.7486	1.8225	1.8223
0.3	1.5600	1.5598	1.6604	1.6602	1.7299	1.7297
0.4	1.4446	1.4444	1.5341	1.5339	1.5976	1.5974
0.5	1.2940	1.2938	1.3707	1.3705	1.4263	1.4261
0.6	1.1083	1.1081	1.1704	1.1702	1.2165	1.2163
0.7	0.8870	0.8868	0.9335	0.9333	0.9689	0.9687
0.8	0.6295	0.6293	0.6600	0.6598	0.6836	0.6834
0.9	0.3344	0.3342	0.3492	0.3490	0.3608	0.3606
1.0	0	0	0	0	0	0

0.001 along radial direction and the time step Δt = 0.00001 which assures the convergence of the obtained numerical solution. It is also observed that reducing the values of $\Delta\xi$ and Δt further does not cause any significant change in the values which results in the stability of the applied numerical techniques. The numerical solutions for shear stress, resistive impedance, velocity, temperature, and concentration distributions for various values of parameters involved in the present study are computed numerically using MATLAB programming. It becomes essential to fix the value of β_1 to find the solution of the equations which should be close to zero as far as possible. In this study, β_1 value is taken as -10^{-30}. If the value of β_1 is taken even 100000 times larger than -10^{-30}, there is no effective change in the obtained shear stress distribution. Hence it is meaningful to fix the value of β_1 as -10^{-30}. The values of other parameters are taken as follows: A_0 = 10, A_1 = 2, A = 2, $\varphi = 10^0$, A_2 = 2, $\beta = 10^0$, δ_s = 0.2, ψ = 0.01, d = 2, L_0 = 2, τ_y = 0.1, M^2 = 3, Gr = 6, Br = 6, Nt = 0.1, Nb = 0.1, Pr = 5, Sc = 12, t = 1, ω = 1, and α^2 = 1.

A tangential force exerted by fluid flow on the wall of the artery created due to the friction between the wall and fluid along the wall is termed as wall shear stress. The shear stress at the wall is highly responsible for changes in the endothelial monolayer. It is significant to note that morphology and spatial orientation of endothelial cell are affected by wall shear stress. It is found from Figs. 2 to 6, the magnitude of wall shear stress (τ_w) is increasing in the upstream of the stenotic region, reaches maximum at the stenotic throat, and is decreasing in the downstream of the stenotic region. The increase in the value of wall shear stress leads to elongation in endothelial cells and causes the cells to align in the direction of flow. At low shear rates, endothelial cells become rounded and have no preferred orientation. From Fig. 2 it is noted that as stenotic height (δ_s) is increased, the magnitude of wall shear stress is increased. In the non-stenotic tapered artery, wall shear stress increases linearly with respect to axial distance. The effect of tapering on wall shear stress has been depicted in Fig. 2. The values for wall shear stress are larger for converging tapered artery than diverging tapered arteries and arteries without tapering and it is seen that the diverging tapered artery possesses lower wall shear stress.

The significant property of Casson fluid is the yield stress. It is a critical value of stress below which blood does not flow. It is a significant property of Casson fluid which helps to overcome the attractive forces between red blood cells and in initiating the flow. From Fig. 3, increase in yield stress (τ_y) and time (t) leads to increase in wall shear stress values. The magnetic field is used to control the flow of blood in human circulatory system. It becomes

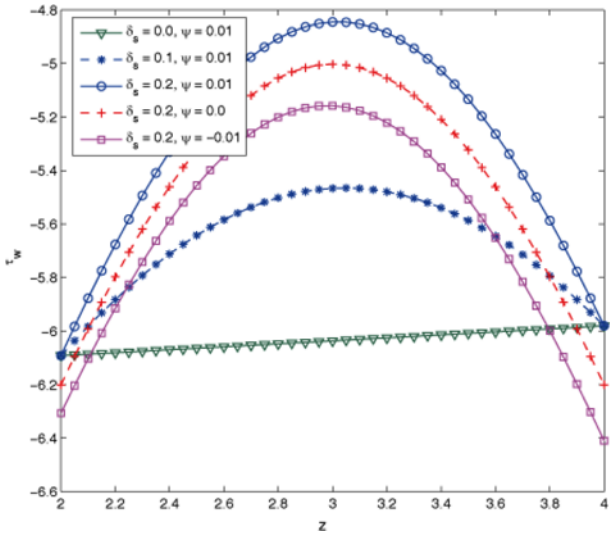

Fig. 2. (Color online) Axial variation of wall shear stress (τ_w) for different values of stenotic height (δ_s) and tapering parameter (ψ).

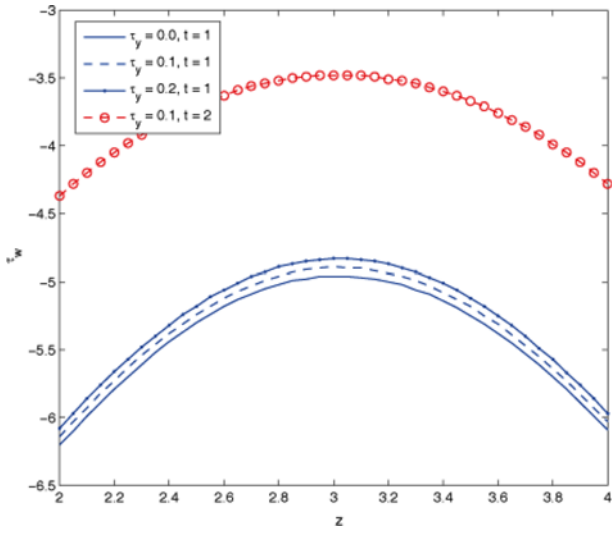

Fig. 3. (Color online) Axial variation of wall shear stress (τ_w) for different values of yield stress (τ_y).

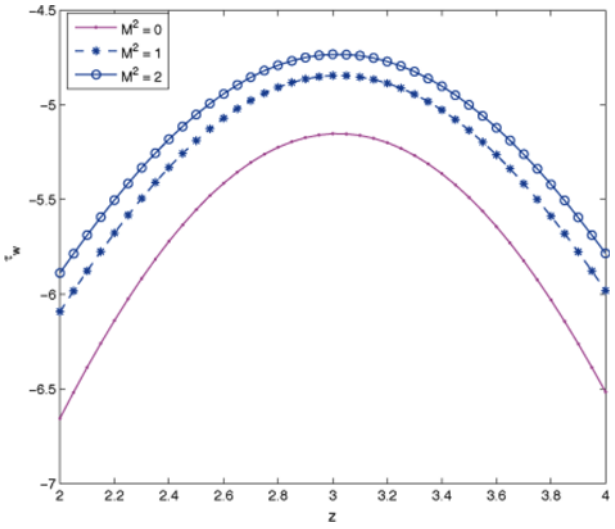

Fig. 4. (Color online) Axial variation of wall shear stress (τ_w) for different values of square of Hartmann number (M).

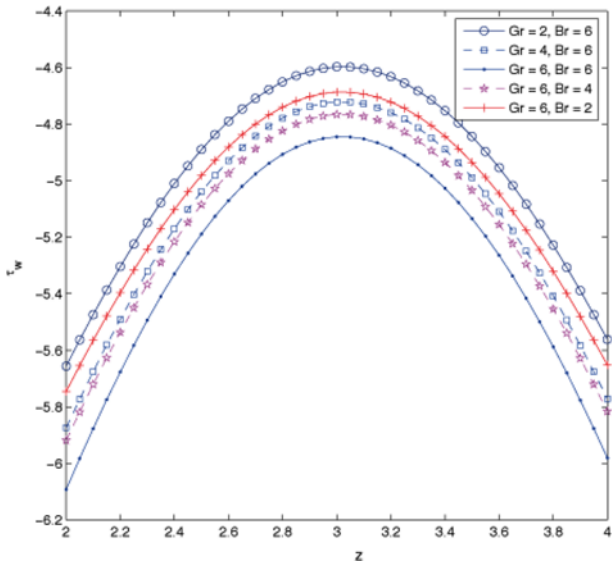

Fig. 5. (Color online) Axial variation of wall shear stress (τ_w) for different values of local temperature Grashof number (Gr) and local nanoparticle Grashof number (Br).

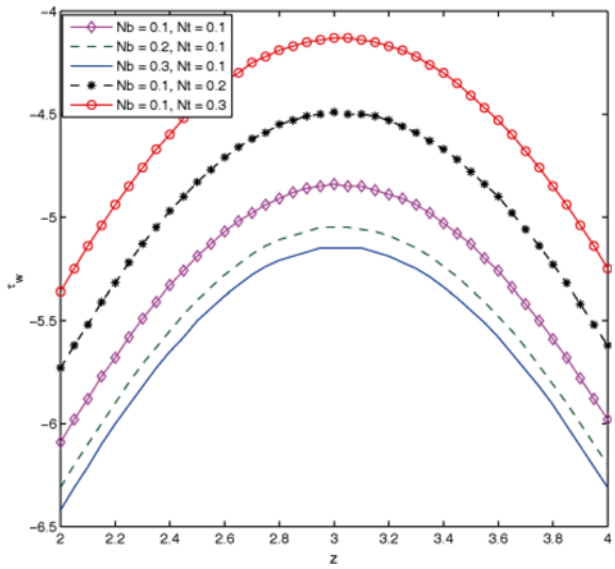

Fig. 6. (Color online) Axial variation of wall shear stress (τ_w) for different values of thermophoresis parameter (Nt) and Brownian motion parameter (Nb).

essential to study the effect of magnetic field on wall shear stress. From Fig. 4, increase in the strength of magnetic field leads to increase in the magnitude of wall shear stress. This is due to the fact that variation of Hartmann number leads to variation of Lorentz force (due to magnetic field) and the Lorentz force produces more resistance to transport phenomena resulting in reduced axial velocity values leading to enhanced wall shear stress values. Grashof number is a dimensionless number which is defined as the ratio of buoyancy to viscous force acting on a fluid. The impacts of local temperature Grashof number (Gr) and local nanoparticle Grashof number (Br) on wall shear stress are illustrated in Fig. 5. The magnitude of wall shear stress decreases with the parameters Gr and Br which can be observed from Fig. 5. Increase in Grashof numbers (Gr and Br) leads to increase in buoyancy force compared to viscous force which tends to accelerate the velocity of fluid resulting in decreased wall shear stress profile. It is evident from Fig. 6 that the magnitude of wall shear stress is enhanced with increase in thermophoresis parameter (Nt). This is due to the fact that increase in the thermophoresis parameter (Nt) leads to increase in thermophoretic force causing the fluid flow to experience higher shear stress at the wall. It is also observed that increase in Brownian motion parameter (Br) increases the random motion of particles in the fluid resulting in decreased wall shear stress.

The axial variations of resistive impedance experienced by the flow of nanofluid for various values of the vital parameters are illustrated in Figs. 7 to 12. The resistance to blood flow is a factor that controls the blood flow rate. It is seen from the figures that the flow resistance values follow an increasing trend. Figure 7 shows the effects of stenotic height (δ_s) and tapering parameter (ψ) on flow resistance. It is significant to note that increased stenotic height results in increased flow resistance and the curve is almost linear in non-stenotic artery. It is also observed that the magnitude of flow resistance values is larger for artery with converging tapering than non-tapered and diverging tapered arteries. From Fig. 8, increase in Hartmann number (M) leads to increase in Lorentz force which opposes the flow resulting in increased resistive impedance. It is examined from Fig. 9 that increase in the parameters A_2, amplitude and β, the inclination angle of the inclined

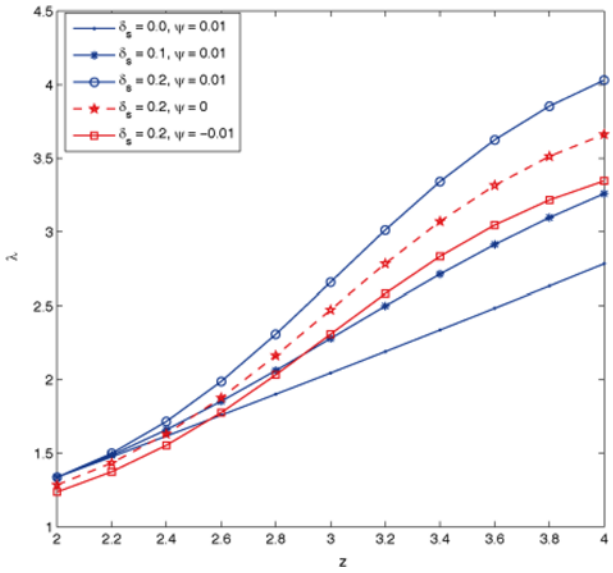

Fig. 7. (Color online) Axial variation of flow resistance (λ) for different values of stenotic height (δ_s) and tapering parameter (ψ).

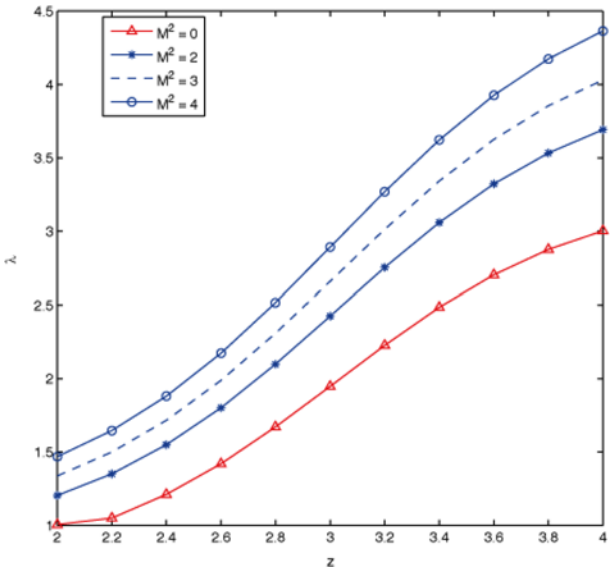

Fig. 8. (Color online) Axial variation of flow resistance (λ) for different values of square of Hartmann number (M).

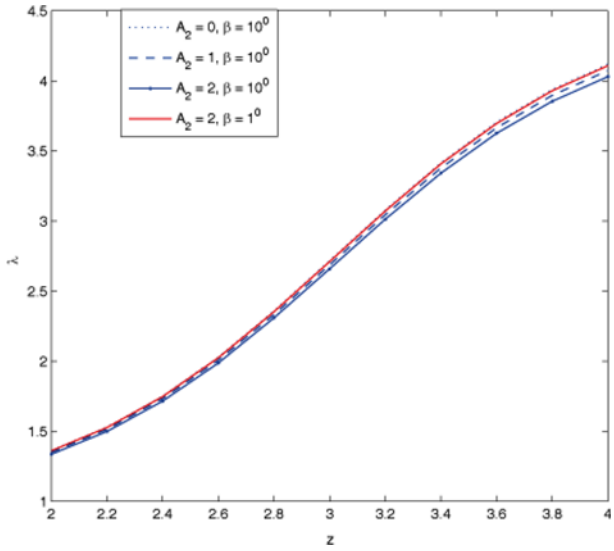

Fig. 9. (Color online) Axial variation of flow resistance (λ) for different values of inclination parameters (A_2 and β).

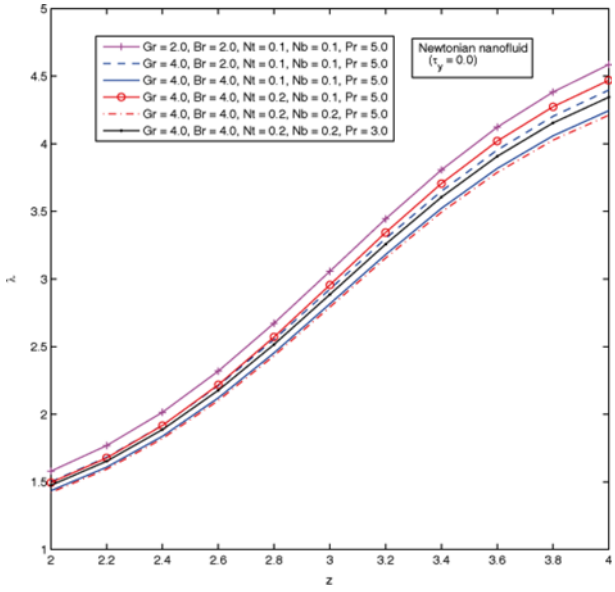

Fig. 10. (Color online) Axial variation of flow resistance (λ) for Newtonian fluid ($\tau_y = 0.0$) for different values of the parameters Gr, Br, Nt, Nb, and Pr.

arteries causes decrease in the flow resistance values.

The combined effects of the local temperature Grashof number (Gr), local nanoparticle Grashof number (Br), thermophoresis parameter (Nt), Brownian motion parameter (Nb), and Prandtl number (Pr) on the axial variation of flow resistance for Newtonian and Casson fluids are illustrated in Figs. 10 to 12. It is observed that when the rheology of blood described as Newtonian or Casson fluid, the increase in the values of parameters Gr, Br, Nb, and Pr leads to a significant decrease in the flow resistance while it is increased with the increase in the thermophoresis parameter (Nt) and yield stress (τ_y). When the rheology of blood is changing from Newtonian fluid (τ_y = 0) to Casson fluid (τ_y = 0.1 and 0.2), the percentage of decrease in the flow resistance due to the increase in the parameters Gr, Br, Nb, and Pr is found to be higher. The sensitivity of Prandtl number (Pr) is weak as compared to other parameters (Br, Gr, and Nb) in the sense that it brings less percentage decrease in the flow resistance for the case of Casson fluid. Another important result is that the percentage increase in the flow resistance with the increase in Nt is found to be higher in the case of blood as Casson fluid rather than that of Newtonian fluid.

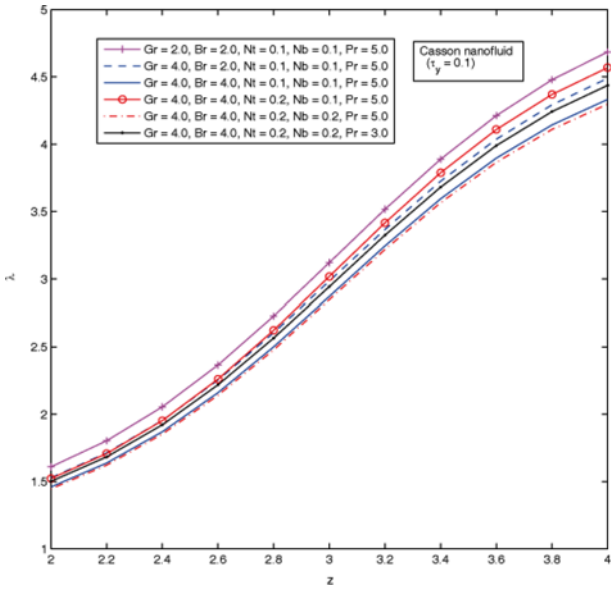

Fig. 11. (Color online) Axial variation of flow resistance (λ) for Casson fluid ($\tau_y = 0.1$) for different values of the parameters *Gr*, *Br*, *Nt*, *Nb*, and *Pr*.

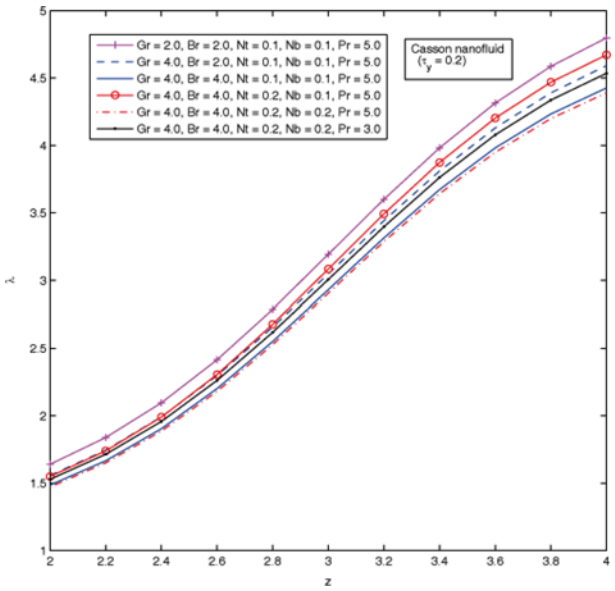

Fig. 12. (Color online) Axial variation of flow resistance (λ) for Casson fluid ($\tau_y = 0.2$) for different values of the parameters *Gr*, *Br*, *Nt*, *Nb*, and *Pr*.

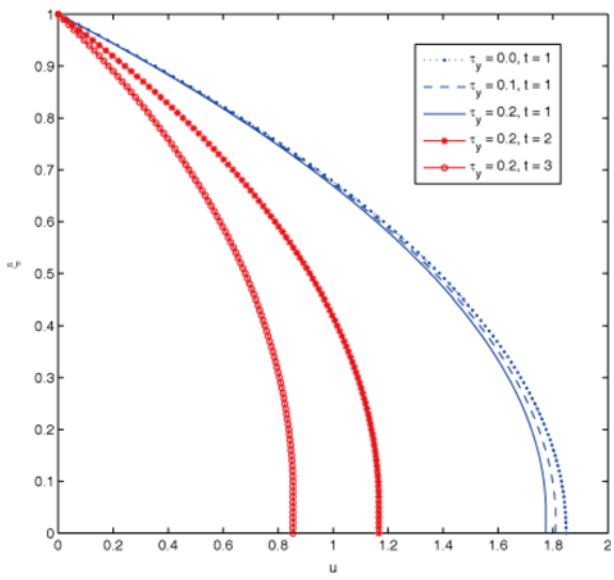

Fig. 13. (Color online) Radial variation of velocity distribution (u) for different values of yield stress (τ_y) and time (t) at the midpoint (z = 5.0) of stenotic region.

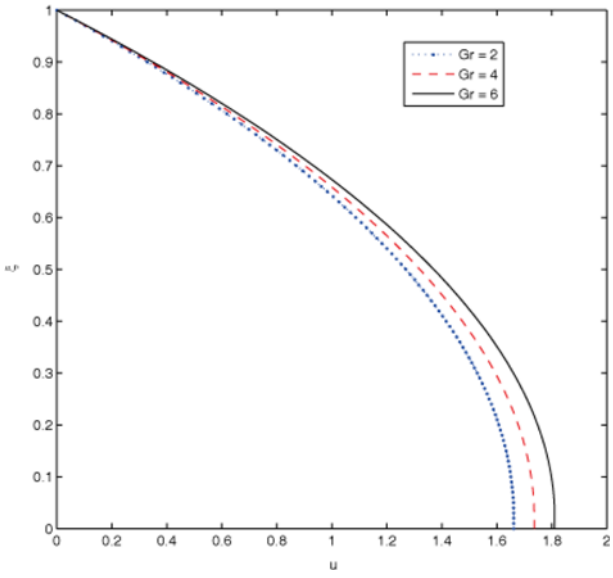

Fig. 14. (Color online) Radial Variation of velocity (u) along axial direction for different values of local temperature Grashof number (*Gr*) at the midpoint (z = 5.0) of stenotic region.

The axial variations of velocity distribution along axial direction for different values of yield stress (τ_y), time (t), local temperature Grashof number (*Gr*), and local nanoparticle Grashof number (*Br*) are illustrated in Fig. 13 to 15. The magnitude of axial velocity decreases with increase in yield stress (τ_y) and with the advancement of time (t) which can be seen in Fig. 13. From Figs. 14 and 15, it is pertinent to note that increase in the parameters, the local temperature Grashof number (*Gr*) and local nanoparticle Grashof number (*Br*), lead to increment in the axial velocity profile. Hence the Casson fluid parameter, yield stress, becomes essential in controlling the velocity of blood.

The influences of thermophoresis parameter (*Nt*) and Brownian motion parameter (*Nb*) on temperature profile (T) are depicted in Figs. 16 to 18 and it can be detected from Figs. 16 and 17 that the temperature distribution increases with the parameters *Nt* and *Nb*. The Brownian motion and thermophoresis phenomenon create additional

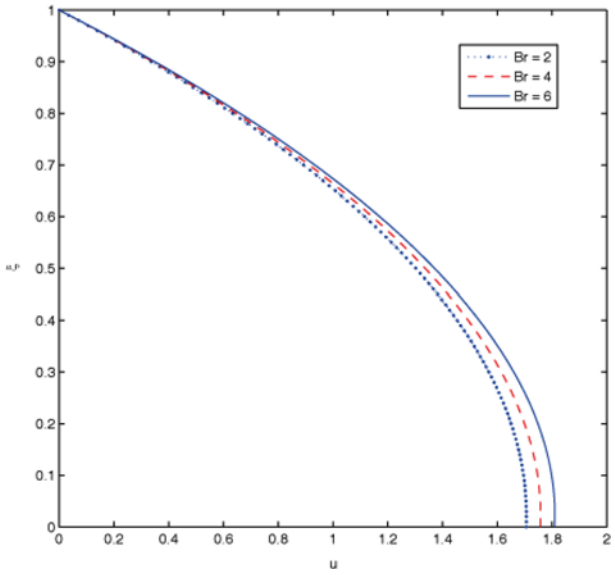

Fig. 15. (Color online) Radial variation of velocity distribution (u) for different values of local nanoparticle Grashof number (Br) at the midpoint (z = 5.0) of stenotic region.

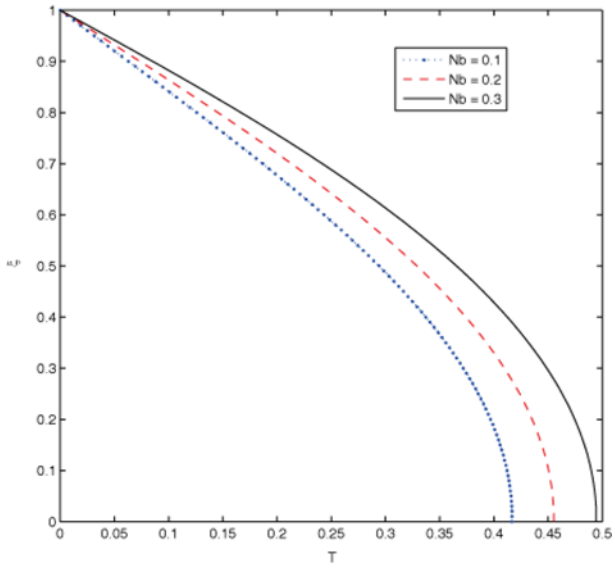

Fig. 17. (Color online) Radial variation of temperature profile (T) for different values of Brownian motion parameter (Nb) at the midpoint (z = 5.0) of stenotic region.

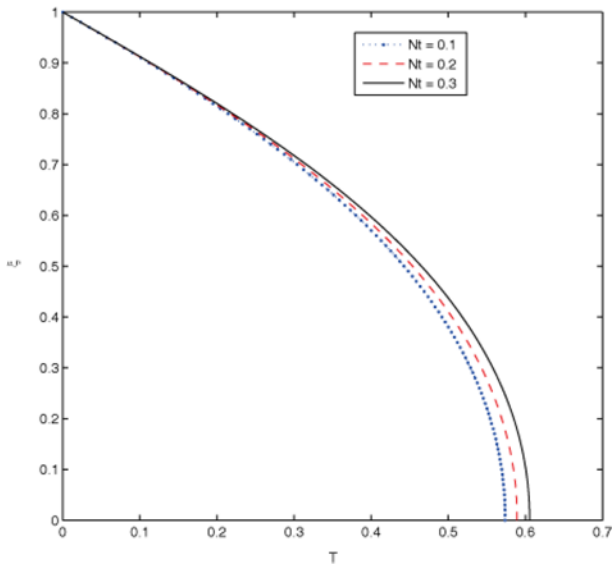

Fig. 16. (Color online) Radial variation of temperature profile (T) for different values of thermophoresis parameter (Nt) at the midpoint (z = 5.0) of stenotic region.

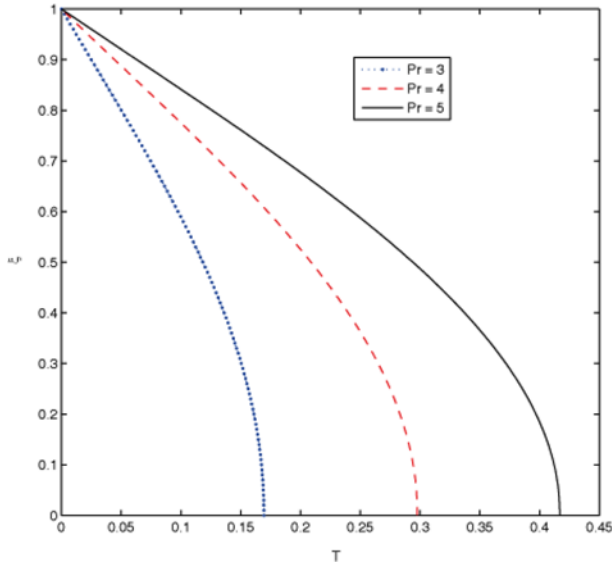

Fig. 18. (Color online) Radial variation of temperature profile (T) for different values of Prandtl number (Pr) at the midpoint (z = 5.0) of stenotic region.

heating by interaction of nanoparticles and the fluid increasing the temperature within the fluid. It is well known that different nanoparticles have different values of Nt and Nb, which leads to have different heat transfer rate. These two parameters are useful to control the heat transfer rate in a nanofluid. It is significant to note from Fig. 18 that increase in the values of Prandtl number causes an effective increase in the temperature.

Figures 19 to 21 depict the radial variation of concentration profiles (C) for various values of the parameters in the model. In Fig. 19, it is shown that the influence of the parameter Nt on the nanoparticle concentration profile is of opposite behaviour as that on the temperature distribution. From Fig. 20, it is observed that as Nb increases, the concentration of nanoparticles also increases. This is due to the fact that an active movement of nanoparticles leads to increase in the density of fluid resulting in increased mass flux and hence the concentration profile increases. The Schmidt number plays significant role in increasing the concentration parameter which can be found from Fig. 21.

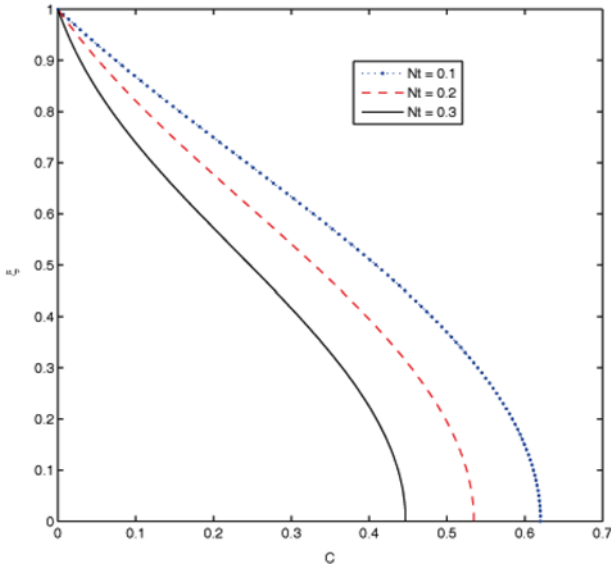

Fig. 19. (Color online) Radial variation of concentration profile (C) for different values of thermophoresis parameter (Nt) at the midpoint (z = 5.0) of stenotic region.

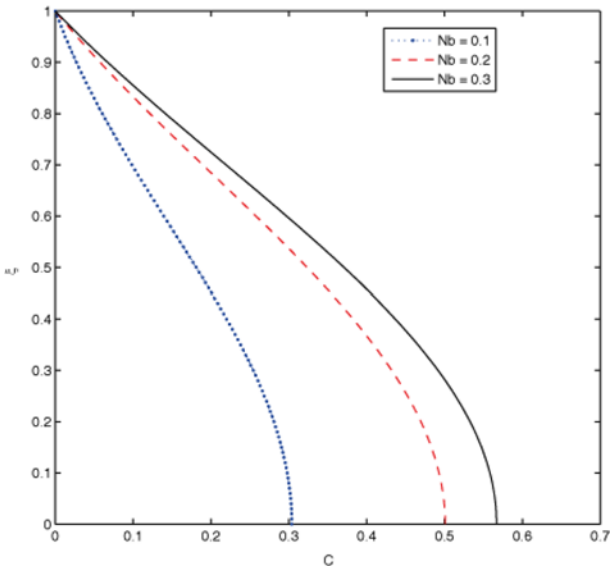

Fig. 20. (Color online) Radial variation of concentration profile (C) for different values of Brownian motion parameter (Nb) at the midpoint (z = 5.0) of stenotic region.

6. Conclusion

This paper brings out the essence of heat and mass transfer on the pulsatile flow of a Casson nanofluid through an inclined tapered arteries with stenosis. It is observed that the wall shear stress and flow resistance increase with the parameters stenotic height, yield stress, Hartmann number while decrease with local temperature Grashof number and local nanoparticle Grashof number. The combined effects of the local temperature Grashof number (Gr), local nanoparticle Grashof number (Br), thermophoresis parameter (Nt), Brownian motion parameter (Nb), and Prandtl number (Pr) on the axial variation of flow resistance for blood as Newtonian fluid and as a Casson fluid are analysed and it is significant to note that the percentage of decrease in the flow resistance with increase in the parameters Gr, Br, Nb, and Pr is higher in the case of blood treated as Casson fluid. The parameters such as yield stress and Hartmann number play significant role in reducing the velocity of blood flow. This result is much useful in medical applications since controlling blood flow is essential during surgeries. It is seen that the temperature profile increases with respect to increase in thermophoresis parameter and Brownian motion parameter. The effects of thermophoresis parameter on concentration profile is conflicting the Brownian motion parameter effect. The Prandtl number and Schmidt number play a predominant role in increasing values of the temperature and the concentration of nanoparticles, respectively. It is noted that the values of wall shear stress and resistive impedance are considerably enhanced in converging tapered arteries than non-tapered and diverging tapered arteries. The results obtained in the present study are practically significant and hence can be applied in treating several diseases by modifying the properties of nanoparticles which are used as drug delivery vehicles in numerous biomedical applications.

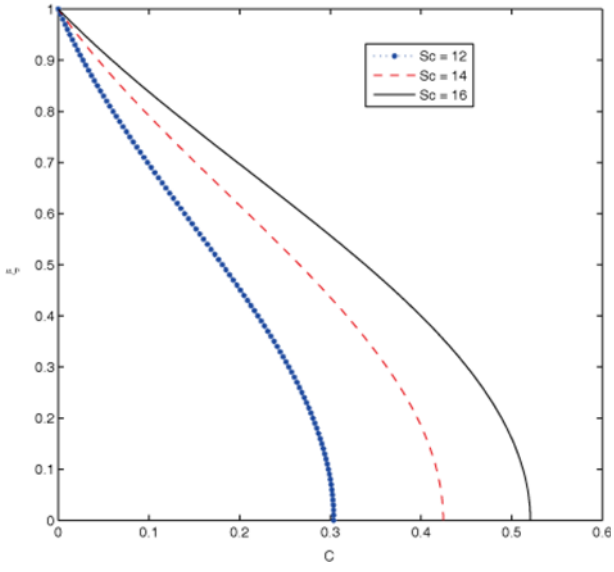

Fig. 21. (Color online) Radial variation of concentration profile (C) for different values of Schmidt number (Sc) at the midpoint (z = 5.0) of stenotic region.

Acknowledgement

Ms. S. Priyadharshini is grateful to the Ministry of Human Resource Development (MHRD), the Government

of India for granting research fellowship.

List of Symbols

Dimensional

$\bar{A}$: Amplitude of body acceleration
$\bar{A}_0$: Amplitude of steady state pressure gradient
$\bar{A}_1$: Amplitude of pulsatile pressure gradient
$\bar{B}_0$: Strength of magnetic field
$\bar{C}$: Concentration of nanoparticles
$\bar{C}_0$: Initial concentration
$\bar{C}_1$: Concentration at the wall
$\bar{c}$: Volumetric expansion coefficient
$D_{\bar{B}}$: Brownian diffusion coefficient
$D_{\bar{T}}$: Thermospheric diffusion coefficient
$\bar{d}$: Location of stenosis
$\bar{F}(\bar{t})$: Periodic body acceleration
$\bar{f}$: Frequency of heart pulse
$\bar{f}_1$: Frequency of body acceleration
$\bar{g}$: Acceleration due to gravity
$\bar{J}_2$: Rate of strain tensor invariant
$\bar{k}_f$: Effective thermal conductivity of fluid
$\bar{L}_0$: Stenotic length
$\bar{p}$: Pressure
$\bar{R}(\bar{z})$: Radius of stenosed artery with tapering
$\bar{R}_p$: Plug core radius
$\bar{r}$: Radial distance
$\bar{T}$: Temperature of fluid
$\bar{T}_0$: Initial temperature
$\bar{T}_1$: Temperature at the wall
$\bar{t}$: Time
$\bar{u}$: Axial velocity
$\bar{v}$: Radial velocity
$\bar{z}$: Axial distance
$\bar{\alpha}$: Thermal diffusivity of fluid
$\bar{\alpha}_c$: Coefficient of thermal expansion
$\bar{\alpha}_t$: Coefficient of thermal expansion with nanoconcentration
$\bar{\delta}_s$: Maximum stenotic height
$\bar{\mu}_c$: Casson's viscosity
$\bar{\mu}(\bar{J}_2)$: Apparent viscosity
$\bar{\rho}_f$: Density of fluid
$\bar{\sigma}$: Electrical conductivity of fluid
$\bar{\tau}_{rz}$, $\bar{\tau}_{zz}$, $\bar{\tau}_{rr}$, $\bar{\tau}_{\theta\theta}$: Stress components
$\bar{\tau}_y$: Yield stress
$\bar{\omega}$, $\bar{\omega}_1$: Angular frequencies

Non-dimensional

A_2 : Amplitude of inclination angle
Br : Local nanoparticle Grashof number
Gr : Local temperature Grashof number
M : Hartmann number
Nb : Brownian motion parameter
Nt : Thermophoresis parameter
Pr : Prandtl number
Re : Reynolds number
ψ : Tapering parameter
Sc : Schmidt number
α_2 : Pulsatile Reynolds number (or Womersley number)
β : Inclination angle
ϕ_1 : Taper angle
λ : Flow resistance (or resistive impedance
τ : Shear stress
τ_w : Wall shear stress

References

Akbar, N.S., 2015, Influence of magnetic field on peristaltic flow of a Casson fluid in an asymmetric channel: Application in crude oil refinement, *J. Magn. Magn. Mater.* **378**, 463-468.

Akbar, N.S. and A.W. Butt, 2015, Magnetic field effects for copper suspended nanofluid venture through a composite stenosed arteries with permeable wall, *J. Magn. Magn. Mater.* **381**, 285-291.

Bali, R. and U. Awasthi, 2012, A Casson fluid model for multiple stenosed artery in the presence of magnetic field, *Appl. Math.* **3**, 436-441.

Beg, O.A., T.A. Beg, R. Bhargava, S. Rawat, and D. Tripathi, 2012, Finite element study of transient pulsatile magnetohemodynamic non-Newtonian flow and drug diffusion in a porous medium channel, *J. Mech. Med. Biol.* **12**, 1250081.

Blair, G.W.S., 1959, An equation for the flow of blood, plasma and serum through glass capillaries, *Nature* **183**, 613-614.

Blair, G.W.S. and D.C. Spanner, 1974, *An Introduction to Biorheology*, Elsevier Scientific, Amsterdam.

Bloch, E.H., 1962, A quantitative study of the hemodynamics in the living microvascular system, *Dev. Dyn.* **110**, 125-153.

Caro, C.G., 1982, Arterial fluid mechanics and atherogenesis, *Clin. Hemorheol. Microcirc.* **2**, 131-136.

Chakravarty, S. and P.K. Mandal, 2000, Two-dimensional blood flow through tapered arteries under stenotic conditions, *Int. J. Non-Linear Mech.* **35**, 779-793.

Charm, S. and G. Kurland, 1965, Viscometry of human blood for shear rates of 0-100,000 sec^{-1}, *Nature* **206**, 617-618.

Chaturani, P. and R. Ponnalagarsamy, 1984, Analysis of pulsatile blood flow through stenosed arteries and its applications to cardiovascular diseases, *Proceedings of the 13th National Conference on Fluid Mechanics and Fluid Power*, Tiruchirapalli, India, 463-468.

Chaturani, P. and R. Ponalagusamy, 1986, Pulsatile flow of Casson's fluid through stenosed arteries with applications to blood flow, *Biorheology* **23**, 499-511.

Chaturani, P. and V. Palanisamy, 1990, Casson fluid model for pulsatile flow of blood under periodic body acceleration, *Biorheology* **27**, 619-630.

Choi, S.U.S. and J.A. Eastman, 1995, Enhancing thermal conductivity of fluids with nanoparticles, *ASME International Mechanical Engineering Congress and Exposition*, San Francisco, California, 44144.

Dash, R.K., K.N. Mehta, and G. Jayaraman, 1996, Casson fluid flow in a pipe filled with a homogeneous porous medium, *Int. J. Eng. Sci.* **34**, 1145-1156.

El-Shahed, M., 2003, Pulsatile flow of blood through a stenosed porous medium under periodic body acceleration, *Appl. Math. Comput.* **138**, 479-488.

Ellahi, R., 2013, The effects of MHD and temperature dependent viscosity on the flow of non-Newtonian nanofluid in a pipe: Analytical solutions, *Appl. Math. Model.* **37**, 1451-1467.

Ellahi, R., M. Hassan, and A. Zeeshan, 2016, A study of heat transfer in power law nanofluid, *Therm. Sci.* **20**, 2015-2026.

Ellahi, R., S.U. Rahman, S. Nadeem, and N.S. Akbar, 2014, Blood flow of nanofluid through an artery with composite stenosis and permeable walls, *Appl. Nanosci.* **4**, 919-926.

Elshehawey, E.F., E.M.E. Elbarbary, N.A.S. Afifi, and M. El-Shahed, 2000, Pulsatile flow of blood through a porous mediumunder periodic body acceleration, *Int. J. Theor. Phys.* **39**, 183-188.

Hariri, S., M. Mokhtari, M.B. Gerdroodbary, and K. Fallah, 2017, Numerical investigation of the heat transfer of a ferrofluid inside a tube in the presence of a non-uniform magnetic field, *Eur. Phys. J. Plus* **132**, 65.

Hayat, T., R. Sajjad, A. Alsaedi, T. Muhammad, and R. Ellahi, 2017, On squeezed flow of couple stress nanofluid between two parallel plates, *Results Phys.* **7**, 553-561.

Ibrahim, S.M., G. Lorenzini, P.V. Kumar, and C.S.K. Raju, 2017, Influence of chemical reaction and heat source on dissipative MHD mixed convection flow of a Casson nanofluid over a nonlinear permeable stretching sheet, *Int. J. Heat Mass Transf.* **111**, 346-355.

Jeffords, J.V. and M.H. Knisley, 1956, Concerning the geometric shapes of arteries and arterioles: A contribution to the biophysics of health, disease, and death, *Angiology*, **7**, 105-136.

Ku, D.N., 1997, Blood flow in arteries, *Annu. Rev. Fluid Mech.* **29**, 399-434.

Liu, G.T., X.J. Wang, B.Q. Ai, and L.G. Liu, 2004, Numerical study of pulsating flow through a tapered artery with stenosis, *Chin. J. Phys.* **42**, 401-409.

Mamourian, M., K.M. Shirvan, and S. Mirzakhanlari, 2016, Two phase simulation and sensitivity analysis of effective parameters on turbulent combined heat transfer and pressure drop in a solar heat exchanger filled with nanofluid by response surface methodology, *Energy* **109**, 49-61.

Mandal, P.K., 2005, An unsteady of non-Newtonian blood flow through tapered arteries with a stenosis, *Int. J. Non-Linear Mech.* **40**, 151-164.

Mekheimer, K.S. and M.A. EI Kot, 2008, The micropolar fluid model for blood flow through a tapered artery with a stenosis, *Acta Mech. Sin.* **24**, 637-644.

Merrill, E.W., A.M. Benis, E.R. Gilliland, T.K. Sherwood, and E.W. Salzman, 1965, Pressure-flow relations of human blood in hollow fibers at low flow rates, *J. Appl. Physiol.* **20**, 954-967.

Nadeem, S. and S. Ijaz, 2015, Theoretical analysis of metallic nanoparticles on blood flow through stenosed artery with permeable walls, *Phys. Lett. A* **379**, 542-554.

Nadeem, S., S. Ijaz, and M. Adil Sadiq, 2014, Inspiration of induced magnetic field on a blood flow of Prandtl nanofluid model with stenosis, *Curr. Nanosci.* **10**, 753-765.

Nguyen, Q.D. and D.V. Boger, 1992, Measuring the flow properties of yield stress fluids, *Annu. Rev. Fluid Mech.* **24**, 47-88.

Ponalagusamy, R., 1986, *Blood Flow through Stenosed Tube*, Ph.D Thesis, Indian Institute of Technology Bombay.

Ponnalagarsamy, R. and M. Kawahara, 1989, A finite element analysis of laminar unsteady flow of viscoelastic fluids through channels with non-uniform cross-sections, *Int. J. Numer. Methods Fluids* **9**, 1487-1501.

Ponalagusamy, R. and R. Tamil Selvi, 2013, Blood flow in stenosed arteries with radially variable viscosity, peripheral plasma layer thickness and magnetic field, *Meccanica* **48**, 2427-2438.

Rahman, S.U., R. Ellahi, S. Nadeem, and Q.M. Zaigham Zia, 2016, Simultaneous effects of nanoparticles and slip on Jeffrey fluid through tapered artery with mild stenosis, *J. Mol. Liq.* **218**, 484-493.

Rashidi, S., J.A. Esfahani, and R. Ellahi, 2017, Convective heat transfer and particle motion in an obstructed duct with two side by side obstacles by means of DPM model, *Appl. Sci.* **7**, 431.

Rodkiewicz, C.M., P. Sinha, and J.S. Kennedy, 1990, On the application of a constitutive equation for whole human blood, *J. Biomech. Eng.-Trans. ASME* **112**, 198-206.

Sharma, M.K., K. Bansal, and S. Bansal, 2012, Pulsatile unsteady flow of blood through porous medium in a stenotic artery under the influence of transverse magnetic field, *Korea-Aust. Rheol. J.* **24**, 181-189.

Shaw, S., P.V.S.N. Murthy, and S.C. Pradhan, 2010, The effect of body acceleration on two dimensional flow of Casson fluid through an artery with asymmetric stenosis, *Open Transport Phenom. J.* **2**, 55-68.

Shaw, S., R.S.R. Gorla, P.V.S.N. Murthy, and C.O. Ng, 2009, Pulsatile Casson fluid flow through a stenosed bifurcated artery, *Int. J. Fluid Mech. Res.* **36**, 43-63.

Shehzad, N., A. Zeeshan, R. Ellahi, and K. Vafai, 2016, Convective heat transfer of nanofluid in a wavy channel: Buongiorno's mathematical model, *J. Mol. Liq.* **222**, 446-455.

Sheikholeslami, M., Q.M. Zaigham Zia, and R. Ellahi, 2016, Influence of induced magnetic field on free convection of nanofluid considering Koo-Kleinstreuer-Li (KKL) correlation, *Appl. Sci.* **6**, 324.

Shukla, J.B., R.S. Parihar, and B.R.P. Rao, 1980, Effects of stenosis on non-Newtonian flow of the blood in an artery, *Bull. Math. Biol.* **42**, 283-294.

Siddiqui, S.U., N.K. Verma, S. Mishra, and R.S. Gupta, 2009, Mathematical modelling of pulsatile flow of Casson's fluid in arterial stenosis, *Appl. Math. Comput.* **210**, 1-10.

Young, D.F., 1968, Effect of a time-dependent stenosis on flow through a tube, *J. Eng. Ind.-Trans. ASME* **90**, 248-254.

Young, D.F., 1979, Fluid mechanics of arterial stenoses, *J. Biomech. Eng.-Trans. ASME* **101**, 157-175.

Young, D.F. and F.Y. Tsai, 1973, Flow characteristics in models of arterial stenoses - I. Steady flow, *J. Biomech.* **6**, 395-402.

Zaman, A., N. Ali, and M. Sajid, 2017, Numerical simulation of pulsatile flow of blood in a porous-saturated overlapping stenosed artery, *Math. Comput. Simul*. **134**, 1-16.